

# Superior Performance and Stability of 2D Dion–Jacobson Halide Perovskite Photodetectors Operated under Harsh Conditions without Encapsulation

Zhengxun Lai, Fei Wang, You Meng, Xiuming Bu, Xiaolin Kang, Quan Quan, Wei Wang, Chuntai Liu, SenPo Yip, and Johnny C. Ho\*

The practical utilization of electronic and optoelectronic materials such as perovskites not only relies on their good device performance and moisture stability but also requires stability under other operating conditions. Herein, the operational stability of the Dion–Jacobson perovskite (DJP) photodetector under different harsh conditions is carefully studied and compared with that of its widely studied counterpart, i.e., the Ruddlesden–Popper perovskite (RPP) photodetector. The DJP-based photodetector can maintain its responsivity after storage in humid environments for two months and can ensure stable operation without any photocurrent degradation under continuous light illumination for 20 000 s. Moreover, the DJP film does not exhibit any changes in its absorbance spectrum and surface morphology when it is heated at 100 °C for 18 h, and the film is hardly affected by high-energy electron beam irradiation. In addition, the mechanical stability of the DJP film is also found to be superior based on the cyclic bending measurements of the fabricated flexible photodetectors. The excellent performance and stability of the DJP-based photodetector are found to be the result of the elimination of weak van der Waals bonds among the octahedral  $\text{PbI}_4$  layers of DJP films, which is typically observed in RPP films.

with the photoelectric performance of these OIHP devices being close to satisfactory and adequate for commercial use. However, the poor stability of OIHPs under humidity, heating, illumination, electron beam irradiation, and mechanical bending inevitably hinders their practical utilization.<sup>[10–17]</sup> To tackle the stability-related problems pertaining to humidity stress, bulky organic molecules such as  $\text{C}_6\text{H}_5(\text{CH}_2)_2\text{NH}_3^+$  (phenethylammonium, PEA),  $\text{CH}_3(\text{CH}_2)_3\text{NH}_3^+$  (butylamine, BA), or isobutylamine (iBA) are introduced into  $\text{MAPbI}_3$  to replace the relatively hydrophilic constituent of  $\text{MA}^+$ .<sup>[18–22]</sup> As shown in Figure 1, two bulky organic molecules, which act as spacer cations, are inserted into the metal halide octahedral layers of 3D perovskites. The binding forces between the spacer cations are van der Waals interactions (red dotted lines in Figure 1). This new type of halide perovskites with a layered quasi-2D structure is known as Ruddlesden–Popper perovskites (RPPs).


Chen et al. improved the stability of perovskite solar cells by growing 2D RPP  $\text{PEA}_2\text{PbI}_4$  capping layers on top of a 3D perovskite film.<sup>[23]</sup> Liu et al. reported the stabilization of a desired  $\alpha\text{-FAPbI}_3$  perovskite phase by protecting it with a quasi-2D  $(\text{iBA})_2\text{FAPb}_2\text{I}_7$  overlayer. Although RPPs can improve the moisture stability of OIHPs to some extent, the stability of RPPs in other ambient environments is not sufficient; in some of these environments, the stability of RPPs is even poorer than that of 3D OIHPs. More notably, the thermal stability of

## 1. Introduction

Organic–inorganic halide perovskites (OIHPs) such as  $\text{MAPbI}_3$  have been widely studied worldwide in recent years owing to their fascinating properties.<sup>[1–5]</sup> For instance, the power conversion efficiency of OIHP-based solar cells is being rapidly enhanced and is approaching that of single-crystal silicon solar cells.<sup>[6,7]</sup> In addition, considerable progress has been made in the development of OIHP-based photodetectors and LEDs,<sup>[8,9]</sup>

Z. X. Lai, F. Wang, Y. Meng, X. M. Bu, X. Kang, Q. Quan, W. Wang, J. C. Ho  
Department of Materials Science and Engineering  
City University of Hong Kong  
Hong Kong 999077, China  
E-mail: johnnyho@cityu.edu.hk

F. Wang  
State Key Laboratory of Luminescence and Applications  
Changchun Institute of Optics, Fine Mechanics and Physics  
Chinese Academy of Sciences  
Changchun 130021, China

 The ORCID identification number(s) for the author(s) of this article can be found under <https://doi.org/10.1002/adom.202101523>.

F. Wang, W. Wang, J. C. Ho  
State Key Laboratory of Terahertz and Millimeter Waves  
City University of Hong Kong  
Hong Kong 999077, China

C. Liu  
Key Laboratory of Advanced Materials Processing & Mold  
(Zhengzhou University)  
Ministry of Education  
Zhengzhou 450002, China

S. B. Yip, J. C. Ho  
Institute for Materials Chemistry and Engineering  
Kyushu University  
Fukuoka 816–8580, Japan

DOI: 10.1002/adom.202101523

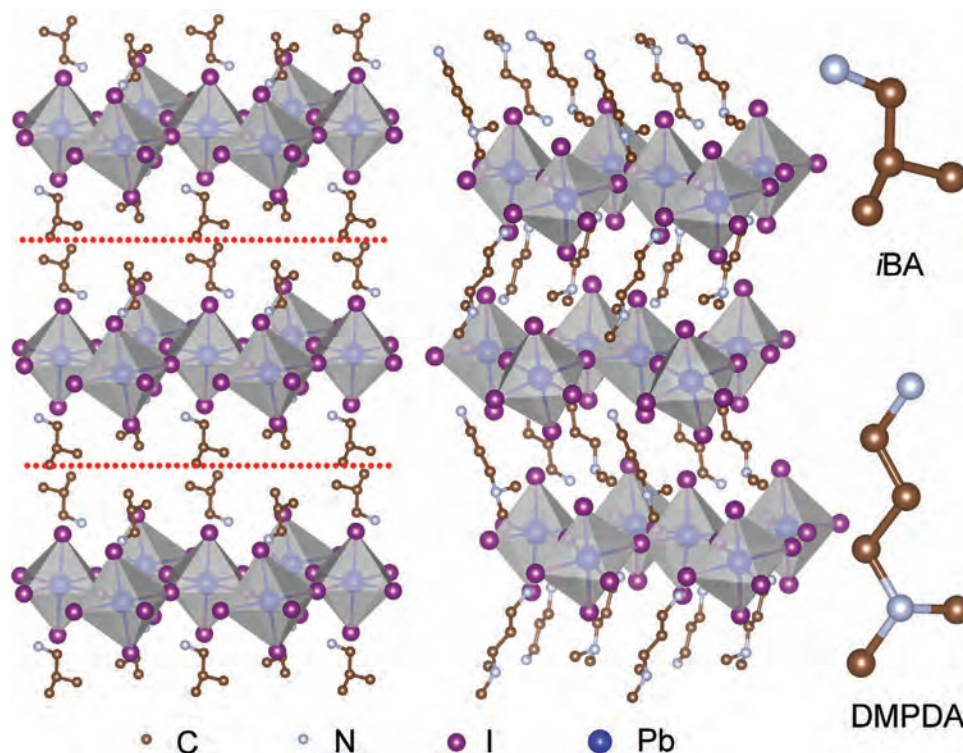


**Figure 1.** Schematic of crystal structures of 2D RPP (left) and DJP (right) films and their corresponding spacer cations.

RPPs has been proven to be fairly weak because bulky organic molecules can easily block the diffusion of heat.<sup>[24]</sup> In addition, the mechanical flexibility of RPPs has been revealed to be poor owing to the existence of weak van der Waals interactions between the spacer cations.<sup>[25]</sup>

Recently, another type of quasi-2D perovskites called Dion–Jacobson perovskites (DJPs) has been proposed, and they have been proven to be more stable in humid environments than RPPs.<sup>[26–29]</sup> In addition, some organic chains in DJPs can considerably enhance the out-of-plane carrier mobility, which is promising for improving the performance of DJPs in electronic devices.<sup>[30]</sup> In contrast to the spacer cations of RPPs, those of DJPs have two amino groups at both ends, as shown in Figure 1. In this arrangement, only one spacer cation is required between the metal halide octahedral layers, and hence, no van der Waals bonds exist in DJPs. It has also been suggested that the presence of van der Waals gaps in RPPs is detrimental to their structural stability, weakening their thermal and moisture stabilities.<sup>[27]</sup> Thus, DJPs are anticipated to be more stable than RPPs in ambient environments. Nevertheless, although the moisture stability of DJPs has been found to be superior recently, their stability under other harsh conditions including high temperatures, intense illumination, electron beam irradiation, and multiple bending has rarely been investigated. Such investigations are essential for the practical application of OIHP-based photoelectric devices. Photoelectric devices routinely reach 65 °C in hot climates under long-term illumination during operation; therefore, they should have good thermal and light illumination stabilities.<sup>[31]</sup> In addition, to ensure that they are suitable for flexible devices, they should have excellent mechanical stability under successive bending.

It is also worth mentioning that OIHPs are highly sensitive to electron beam irradiation.<sup>[32–34]</sup> Because in-depth transmission electron microscopy (TEM) and scanning electron microscopy (SEM) studies are always performed to assess various fundamental properties of OIHPs for subsequent material design and optimization, the stability enhancement of OIHPs under electron beam irradiation is another important enabling factor for their further development and deployment in industry.

In this work, we designed and performed systematic investigations to evaluate the stability of DJPs under the harsh conditions mentioned above. Specifically, 2D DJP films consisting of [DMPDA]PbI<sub>4</sub> (DMPDA = *N,N*-dimethyl-1,3-propanediamine, C<sub>5</sub>H<sub>14</sub>N<sub>2</sub>) were fabricated by a one-step spin-coating method. To ensure a fair comparison, 2D RPP films made of (iBA)<sub>2</sub>PbI<sub>4</sub> and mixed spacer cation films made of 2D iBA(DMPDA)<sub>0.5</sub>PbI<sub>4</sub> (hereinafter denoted as “MIX films” for simplicity) were also prepared. These three types of 2D OIHP films were then configured to form photodetectors, and their optoelectronic properties and stability under different harsh conditions were thoroughly examined. In terms of the optoelectronic properties, the DJP films exhibited higher photocurrent and responsivity than the RPP and MIX films. To determine the stability of the 2D films, moisture stability was first tested. After the films were stored in an ambient environment for two months, no noticeable change was observed in the DJP absorption edge and the responsivity of the DJP-based photodetectors did not decrease. In addition, under continuous chopped-light illumination for 10 000 s, the DJP-based photodetectors produced stable photocurrent without any degradation. The absorbance spectrum and surface morphology of the DJP films also remained the same after being heated at 100 °C for 18 h. Importantly, the DJP films

underwent exposure to 10 kV electron beam irradiation without any surface damage. The mechanical stability of the DJP films was proven to be considerably better than those of the other two films based on cyclic bending measurements. The superior stability of the DJP films under different harsh conditions can be attributed to their stable lattice structure without any weak van der Waals bonds among the octahedral  $\text{PbI}_4$  layers. These results clearly demonstrate the excellent stability of DJPs and provide a clear direction for overcoming the bottlenecks preventing the practical utilization of OIHPs.

## 2. Results and Discussion

The X-ray diffraction (XRD) patterns of the three film samples are shown in Figure S1 in the Supporting Information. The simulated XRD pattern of the DJP film is also shown. The actual XRD peaks of the DJP film fitted well with the simulated ones. The lattice planes of the DJP and RPP films are labeled at the corresponding peaks using black and blue colors, respectively. For the MIX phase, peaks from not only the RPP phase but also the DJP phase were observed, confirming the nature of the mixed spacer cations. The thickness of the films was also acquired from cross-sectional SEM images (Figure S2, Supporting Information) and was found to be 0.9–1  $\mu\text{m}$ . First, the performance of the as-prepared 2D halide perovskite-based photodetectors was characterized, and the planar device structure was configured (Figure S3, Supporting Information). **Figure 2a** shows the on/off switching characteristics of the three devices under chopped-light illumination from a laser (wavelength: 450 nm) under a bias voltage of 1.5 V, and

the results indicate the good switching repeatability and stability of the photodetectors under monochromatic light. The on/off current ratio of the DJP sample was as high as  $2 \times 10^5$ , whereas those of the MIX and RPP samples were determined to be  $3.5 \times 10^4$  and  $1.5 \times 10^4$ , respectively. Figure 2b shows the photocurrents of the devices under different light intensities. The relationship of the photocurrents with the light intensities is sublinear, which is often the case for photodetectors with layered materials. This relationship usually results from the complex processes of electron–hole generation, trapping, and recombination in the films.<sup>[35,36]</sup> Figure 2c shows the corresponding responsivity values ( $R = \frac{I_p}{\Phi S}$ , where  $I_p$  is the photocurrent,  $\Phi$  is the light intensity, and  $S$  is the active area of the photodetector) of the devices under various light intensities. The responsivity of the DJP sample was clearly larger than those of the MIX and RPP samples, and the maximum value was found to be  $74 \text{ mA W}^{-1}$ . In addition, the detectivity ( $D^*$ ) and external quantum efficiency (EQE) of the devices were calculated according to the equations  $D^* = RS^{1/2}/(2eI_d)^{1/2}$  and  $\text{EQE} = hcR/e\lambda$ , where  $e$  is the electronic charge,  $I_d$  is the dark current of the device,  $h$  is Planck's constant,  $c$  is the velocity of light, and  $\lambda$  is the wavelength of the incident light. The  $D^*$  and EQE values of the photodetectors under different light intensities are shown in Figure S4 in the Supporting Information. The  $D^*$  and EQE values of the DJP-based photodetector were determined to be  $1.06 \times 10^{12}$  and 20.4%, respectively; these values provide the DJP-based photodetector with evident advantages over the MIX- and RPP-based photodetectors. Furthermore, the response speed (rise and decay times from 10% to 90% and 90% to 10% of the steady-state photocurrent, respectively) of the DJP-based

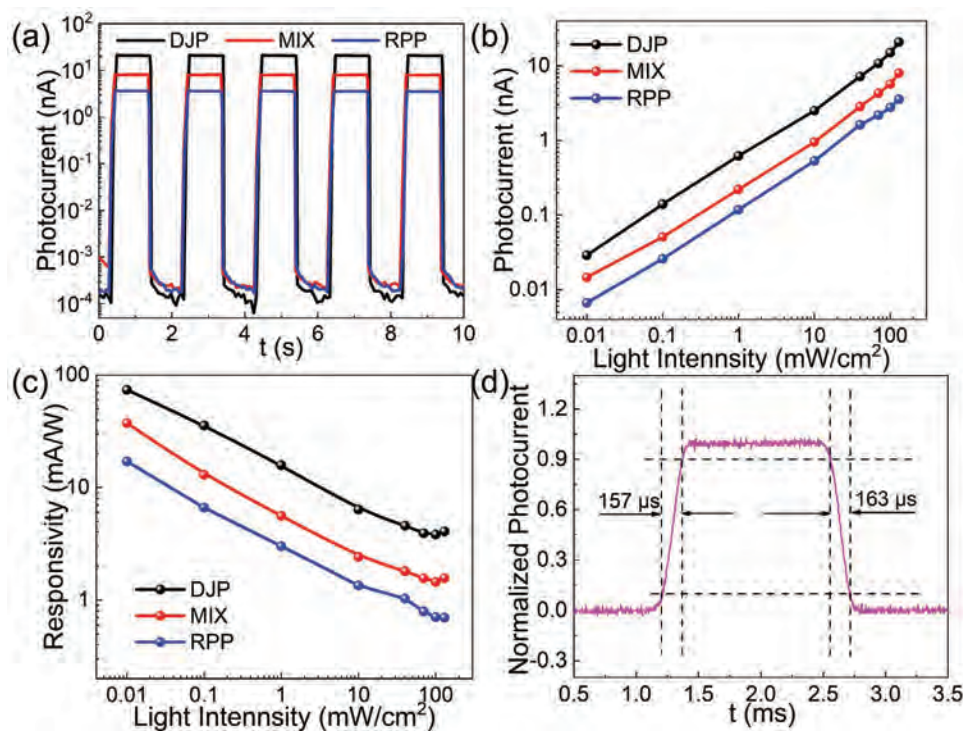


**Figure 2.** a) Time-dependent photocurrent. b) Dependence of photocurrent on light intensity. c) Dependence of responsivity on light intensity. d) Curve of high-resolution current versus time for the DJP film device.

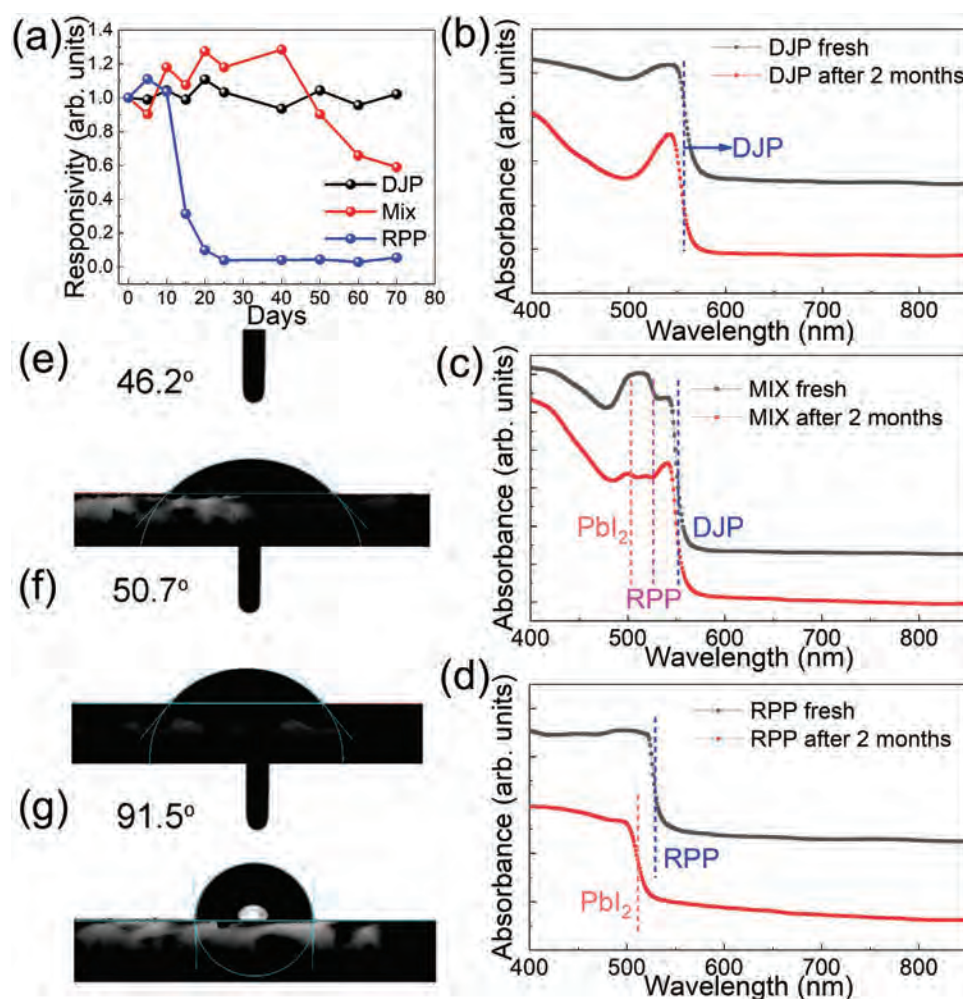


**Figure 3.** a) Normalized responsivities after storage under ambient conditions with humidity of 68% for 25 d. UV-vis absorbance spectra of b) DJP, c) MIX, and d) RPP films before and after storage. Evaluation of water contact angles of e) RPP, f) MIX, and g) DJP films.

photodetector was acquired from the high-resolution photocurrent–time ( $I_p-t$ ) curves shown in Figure 2d, and the rise and decay times were as short as 157 and 163  $\mu$ s, respectively. When the device geometry was the same and the comparison was consistent, the DJP-based photodetector exhibited the best performance among all the photodetectors. A comparison of the performance parameters of some typical 2D halide perovskite-based photodetectors with those of the DJP-based photodetector is presented in Table S1 in the Supporting Information. The performance of the DJP-based photodetector is superior to that of the single-crystal perovskite-based photodetectors.

In addition to the photoelectric performance, device stability is crucial for the practical applications of 2D perovskites. Hence, the long-term moisture stability of the samples was carefully studied. **Figure 3a** shows the changes in the normalized responsivities of the samples after they were stored in an ambient environment with a humidity of 68% without encapsulation. The responsivity of the RPP-based photodetector decreased to 4% of its initial value after 25 d. However, the MIX-based photodetector maintained its initial responsivity even after 40 d but gradually decreased afterward. Interestingly, the responsivity of the DJP-based photodetector did not

show any deteriorating trend even after 70 d of storage without encapsulation. Furthermore, to study the long-term impact of the ambient environment in detail, the absorbance spectra of the fresh films and the films stored in an ambient environment with 68% humidity were measured (Figure 3b–d). There was clearly no change in the absorption edge (552 nm) of the DJP films, confirming their excellent moisture stability. For the MIX film, only the absorption edges of the DJP and RPP phases located at 552 and 526 nm, respectively, could be acquired in the spectrum of the fresh films; this characteristic is attributed to the mixed-phase nature of the film. However, after two months of storage, the absorption edge of the RPP phase was replaced by that of PbI<sub>2</sub> located at 503 nm, whereas the absorption edge of the DJP phase remained unchanged, suggesting the decomposition of the spacer cations in the RPP phase. Similarly, as shown in Figure 3d, the RPP film completely degraded to a PbI<sub>2</sub> film after storage. The superior stability of DJPs in humid environments can be ascribed to the strong hydrophobicity of the spacer cations and the absence of weak van der Waals bonds; the van der Waals interactions between the spacer cations in RPPs harm their structural stability but make them sensitive to humid environments.<sup>[27,28]</sup> Furthermore,

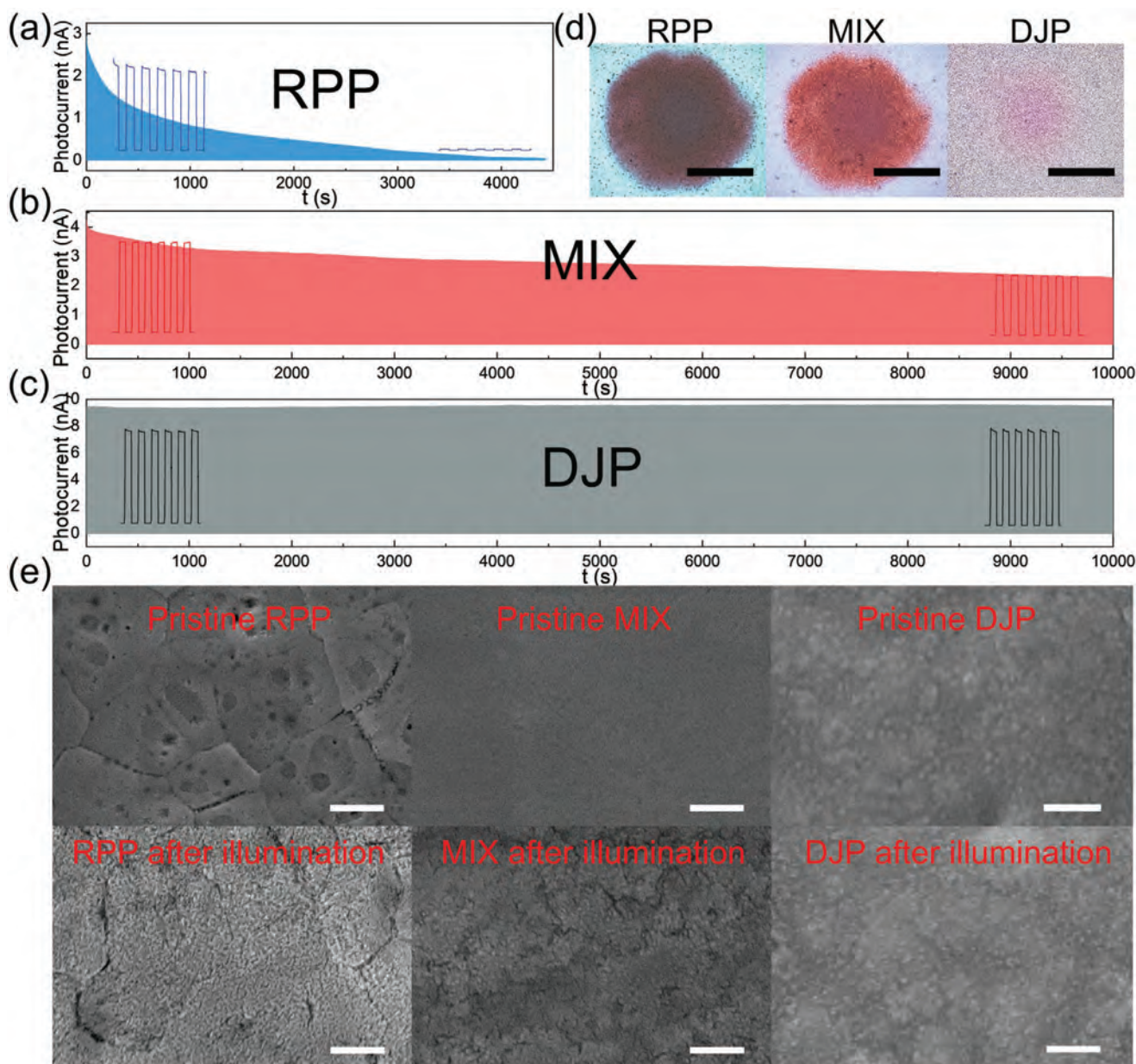


**Figure 4.** On/off switching cycles of a) RPP-, b) MIX-, and c) DJP-based photodetectors under chopped-light illumination from laser with light intensity of  $380 \text{ mW cm}^{-2}$  for 10 000 s. d) Photographs of films after 30 min of illumination (scale bar: 0.5 mm). e) SEM images of three 2D perovskite films before and after laser illumination (scale bar:  $1 \mu\text{m}$ ).

the water contact angles of the three samples were measured (Figure 3e–g). The contact angle of the DJP film was as large as  $91.5^\circ$ , which was considerably larger than those of the MIX ( $50.7^\circ$ ) and RPP ( $46.2^\circ$ ) films, indicating the superior hydrophobicity of the DJP film.

Because photoelectric devices are expected to be operated under continuous illumination, the long-term on/off switching stability of the photodetectors is also important. Accordingly, the on/off switching cycles of the three devices under chopped-light illumination were measured, as shown in Figure 4a–c. The bias voltage was set to 1.5 V, and the light intensity of the 450 nm laser was fixed at  $380 \text{ mW cm}^{-2}$ . Figure 4c indicates that

the photocurrent of the DJP sample was very stable during continuous operation for 10 000 s. In comparison, the photocurrent of the RPP sample was only 1.3% of its initial value after 4500 s and that of the MIX sample deteriorated to 53% of its initial value after the operation. To visually detect the influence of illumination on the 2D perovskites, we placed the three films under continuous illumination from a 450 nm laser with an intensity of  $380 \text{ mW cm}^{-2}$  for 30 min. Optical images of the illuminated areas of the films were then taken. As shown in Figure 4d, the color of the illuminated area of the RPP film changed to dark red, which indicates the destructive effect of illumination. For the MIX sample, illumination generated a

shiny red area, suggesting that the damage was weaker than that in the RPP sample. Strikingly, for the DJP film, illumination causes only a very small area to turn slightly pale pink, which confirms that the influence of illumination on the film is very limited. Furthermore, SEM images of the area before and after illumination were obtained. As shown in Figure 4e, no noticeable change was observed in the surface of the DJP film. In contrast, for the RPP and MIX films, valley-like textures appeared after illumination, which can be attributed to the decomposition of the organic spacer cations because of illumination.<sup>[37]</sup>

OIHP devices should also possess good thermal stability because photoelectric devices are usually required to work in environments where the temperatures are higher than those in indoor environments. To investigate the thermal stability of the films, the three films were heated at 100 °C in a glove box. Figure 5a–c shows the UV–vis absorbance spectra of the films after they were heated for 0–18 h. The intensity of the absorbance spectra of the RPP and MIX films gradually weakened after heating, and the absorption edge of the RPP film eventually vanished. However, no clear change was observed in the absorbance spectrum of the DJP film, suggesting its

superior thermal stability. Moreover, SEM images of the fresh samples and the samples that underwent heating were studied (Figure 5d). Clearly, the morphology of the DJP film remained almost the same. However, the RPP and MIX films transformed into porous films after being heated, which may be due to the decomposition of the organic spacers under continuous heating. This is because the organic components are considerably more sensitive to high temperatures than inorganic  $\text{PbI}_2$ .<sup>[38]</sup> To confirm this, thermogravimetric analysis (TGA) was performed on the 2D OIHP samples in a nitrogen atmosphere (Figure S5, Supporting Information). The RPP and DJP samples exhibited two thermal events. The RPP sample began to crack at 223 °C in the first thermal event and underwent a weight loss of 46% before the second event; this weight loss corresponded to the weight ratio of *i*BAI in the RPP sample. For the DJP sample, the first thermal event started at 265 °C, and 44% of the weight was lost before the second event; this weight loss corresponded to the weight ratio of [DMPDA]<sub>2</sub> in the DJP sample. For the MIX sample, three thermal events were derived from the decomposition of *i*BAI, [DMPDA]<sub>2</sub>, and  $\text{PbI}_2$ . The TGA patterns confirmed that organic spacer cations are crucial to the thermal stability of OIHPs. The DJP sample could

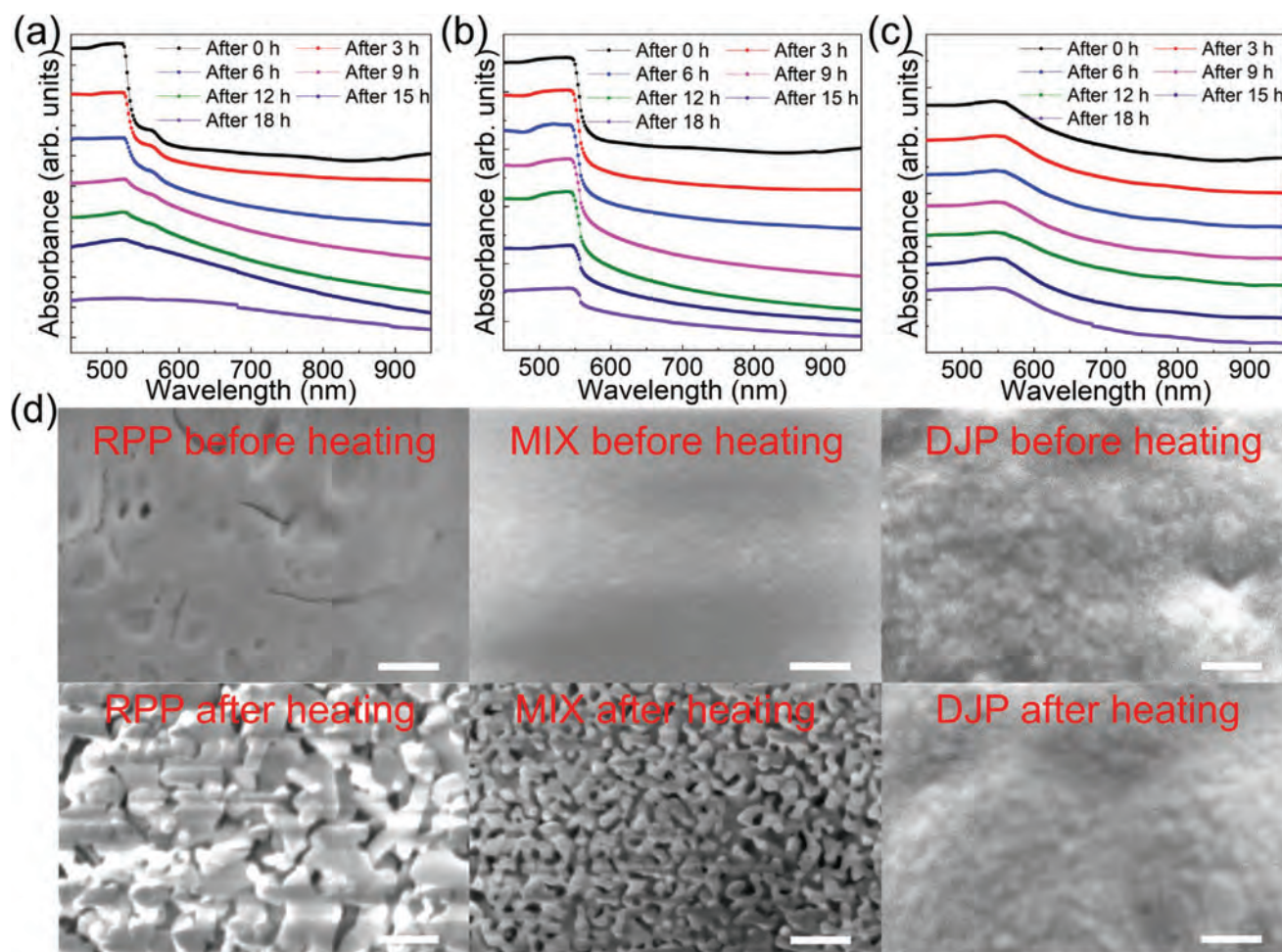


**Figure 5.** a) Absorption spectra of a) RPP, (b) MIX, and c) DJP films after heating for different durations at 100 °C within glove box. d) SEM images of 2D perovskite films before and after thermal heating for 18 h at 100 °C (scale bar: 1 μm).

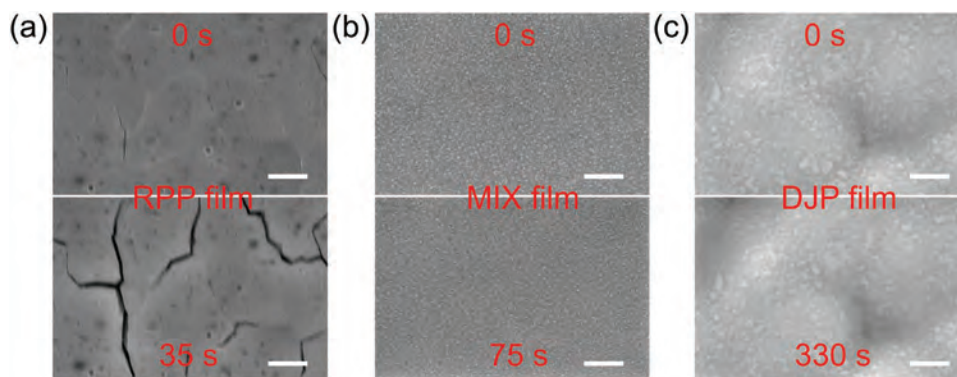


**Figure 6.** SEM images of a) RPP, b) MIX, and c) DJP films before and after exposure to 10 kV electron beam irradiation (scale bar: 1  $\mu\text{m}$ ).

withstand a higher temperature than the RPP sample. To make this observation more explicit, optical images of the fresh films and the films that underwent heating for 18 h were obtained, as shown in Figure S6 in the Supporting Information. There were evident color changes in the RPP and MIX films, but the DJP film maintained its original state. The better thermal stability of the DJP film can be attributed to its enhanced structural stability because of the absence of van der Waals bonds among the octahedral  $\text{PbI}_4$  layers.<sup>[27,39]</sup>

In addition to good stability under the ambient conditions mentioned above, good stability under electron beam irradiation is also important. One of the major reasons for this is that the in-depth study of microscopic properties requires the assistance of SEM and TEM.<sup>[34]</sup> Hence, the impact of electron beam irradiation on 2D perovskite films was investigated by SEM. As shown in Figure 6, SEM images of the RPP, MIX, and DJP films were acquired before and after exposure to the electron beam. For the RPP film, clear cracks were observed, which were caused by the electron beam after only 35 s of exposure. In contrast, for the MIX and DJP films, almost no change was observed after electron beam irradiation. The videos in the Supporting Information further demonstrate the influence of the electron beam on the three films more clearly. The cracks in the RPP film are associated with the rapid volatilization of the organic spacers because of electron beam irradiation, whereby tensile stress was induced on the film surface. Then, cracks appeared and propagated along the grain boundary.<sup>[40]</sup> The DJP

film can survive electron beam irradiation owing to its stable structure, where defects due to the volatilization of the organic cations can hardly occur.<sup>[41]</sup>

For flexible electronic devices, stability under mechanical bending is crucial. Here, DJP-, MIX-, and RPP-based flexible photodetectors were fabricated on flexible polyimide substrates. The photocurrents of the three flexible photodetectors were evaluated as a function of the bending radius (Figure 7a). The measurement setup for evaluating the bending radius (inset of Figure 7b) provided accurate control. The photocurrents of the RPP- and MIX-based photodetectors decreased substantially as the bending radius decreased; only 6% and 12% of their initial values remained, respectively, after they were bent to 2 mm. However, for the DJP-based flexible photodetector, the photocurrent remained unchanged after being bent to 20 mm or even to 10 mm and began to decrease only when the bending radius was lower than 6 mm, indicating the better flexibility of the DJP film. Subsequently, cyclic testing was carried out on the three flexible photodetectors by bending them 2000 times at a bending radius of 4 mm. As shown in Figure 7b, the photocurrent of the RPP-based photodetector started to decrease immediately after being bent and only 24.2% of its initial value remained after 2000 bending cycles. The normalized photocurrent of the MIX-based photodetector also reduced to 30.7% after the same number of bending cycles. For the DJP-based photodetector, the photocurrent maintained 92% of its original value after the same number of bending cycles,

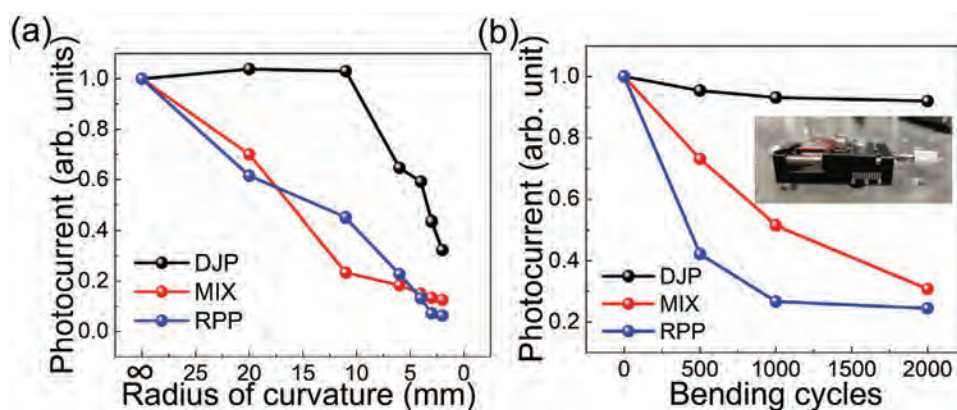


**Figure 7.** Dependence of normalized photocurrent on a) different bending curvatures and b) different bending cycles for 2D perovskite film-based flexible photodetectors.

confirming its superior mechanical flexibility. This remarkable flexibility is anticipated considering the lack of weak van der Waals interactions among the octahedral  $\text{PbI}_4$  layers. The van der Waals bonds in RPP films can easily be broken by an external force; therefore, bending adversely affects their photoelectric performance.

To investigate the weak van der Waals bonds in the 2D perovskite films, pressure-sensitive tape (Scotch Tape), which is widely used in the mechanical exfoliation of 2D materials, was applied to the three sample films. As shown in Figure S7 (Supporting Information), a large area of the RPP film was easily exfoliated by the tape, whereas a small segment of the MIX film was exfoliated. In contrast, the DJP film was not influenced by the tape owing to the strong I–H bond between ammonium and the octahedral  $\text{PbI}_4$  layer, which contributes to its excellent stability.<sup>[42]</sup> These mechanical exfoliation results prove that the binding force in RPP films is very weak and can be readily broken by an external force. Accordingly, humidity, light illumination, heat, electron beam irradiation, and mechanical bending cause considerable harm to RPP-based photoelectric devices. However, DJP films, which do not have weak van der Waals bonds, overcome the limitations of the RPP films and may primarily drive the direction of future development of OIHPS.

### 3. Conclusion

In this study, 2D films consisting of DJP, RPP, and MIX spacer cations were fabricated by a one-step spin-coating method and configured to form photodetectors. The performance of the DJP-based photodetector was superior to that of the RPP- and MIX-based photodetectors. More importantly, the stability of the DJP films was remarkable in all harsh environments and was considerably better than those of the RPP and MIX films. After two months of storage at a humidity of 68%, the responsiveness of the DJP-based photodetector together with the absorbance spectrum of the DJP film could be maintained without any noticeable change. In addition, the surface morphology of the DJP film was hardly affected by light illumination and electron beam irradiation. The photocurrent of the DJP film could be maintained at its initial value after 10 000 s of on/off switching under light illumination. Even after the DJP film was heated at 100 °C for 18 h, its absorbance spectrum did not exhibit any change. The flexibility of the DJP-based photodetector was excellent, with the photocurrent remaining the same after 2000 bending cycles. The absence of weak van der Waals bonds among octahedral  $\text{PbI}_4$  layers is the major reason for the stability of the DJP film in these harsh environments. Our work is expected to pave the way for the study of the stability of optoelectronic materials in different harsh environments and provide a clear direction to overcome the problems causing the poor stability of OIHPS.

### 4. Experimental Section

*Synthesis of Perovskite Precursors:* For the RPP ( $i\text{BA}$ )<sub>2</sub> $\text{PbI}_4$  film,  $i\text{BAI}$ , and  $\text{PbI}_2$  at a molar ratio of 2:1; for the MIX  $i\text{BA}[\text{DMPDA}]_{0.5}\text{PbI}_4$  film,

$i\text{BAI}$ ,  $[\text{DMPDA}]_2$ , and  $\text{PbI}_2$  at a molar ratio of 1:0.5:1; and for the DJP  $[\text{DMPDA}]\text{PbI}_4$  film,  $[\text{DMPDA}]_2$  and  $\text{PbI}_2$  at a molar ratio of 1:1 were dissolved in dimethylformamide, respectively. The solutions were then stirred overnight at room temperature.

*Device Fabrication:* The 2D OIHP films were fabricated by a one-step spin-coating method in a nitrogen-filled glovebox, in which the oxygen and moisture concentrations were well controlled at the parts-per-million level. Glass and polyimide (for flexible photodetectors) substrates were first ultrasonically washed by acetone, ethanol, and deionized water for 15 min in succession. These substrates were then treated with mild oxygen plasma to improve their hydrophilicity. For the fabrication of the films, the precursor solution (30  $\mu\text{L}$ ) was spin-coated on the substrate at 3000 rpm for 30 s, followed by thermal annealing at 100 °C for 10 min to fully crystallize the samples. For the construction of the photodetectors, Au electrodes (thickness: 50 nm) were thermally evaporated onto the films with the assistance of a shadow mask, whose channel length and width were 10 and 70  $\mu\text{m}$ , respectively.

*Film and Device Characterization:* XRD (D2 PHASER with Cu  $K\alpha$  radiation, Bruker) was used to evaluate the crystal structure of the obtained films. The surface morphologies of the 2D OIHP films were characterized by SEM (Quanta 450 FEG, FEI). UV–vis absorption spectra were recorded using a spectrometer (Lambda 25 UV-VIS, PerkinElmer) and a UV–vis–near-infrared spectrophotometer (UH4150, Hitachi). The water contact angles of the films were measured using a contact angle tester (DataPhysics). TGA curves were acquired using a gravimetric analyzer (SDT Q600, TA Instruments) from 25 to 600 °C at a heating rate of 2 °C  $\text{min}^{-1}$  in a nitrogen atmosphere. The electrical performance of the fabricated devices was characterized using a standard electrical probe station and a semiconductor analyzer (4155C, Agilent Technologies, California, USA). A 450 nm laser was used as a light source for the photodetector measurement, and the power of the incident irradiation was measured using a power meter (PM400, Thorlabs). An attenuator was also employed to tune the irradiation power used for illuminating the device. To determine the response time of the photodetectors, a low-noise current amplifier (SR570, Stanford Research Systems, USA) combined with a digital oscillator (TBS1102B-EDU, Tektronix, USA) was used to obtain high-resolution current–time curves.

### Supporting Information

Supporting Information is available from the Wiley Online Library or from the author.

### Acknowledgements

This research was financially supported by the Research Fellow Scheme (RFS2021-1S04) and Theme-based Research Scheme (T42-103/16-N) of the Research Grants Council of Hong Kong SAR, China, and by the Foshan Innovative and Entrepreneurial Research Team Program (2018IT100031).

### Conflict of Interest

The authors declare no conflict of interest.

### Data Availability Statement

The data that support the findings of this study are available from the corresponding author upon reasonable request.



## Keywords

Dion–Jacobson phase, halide perovskites, photodetectors, Ruddlesden–Popper phase, device stability

Received: July 27, 2021

Revised: August 29, 2021

Published online: October 4, 2021

- [1] H. P. Zhou, Q. Chen, G. Li, S. Luo, T. Song, H. S. Duan, Z. R. Hong, J. B. You, Y. S. Liu, Y. Yang, *Science* **2014**, *345*, 542.
- [2] C. Quarti, E. Mosconi, J. M. Ball, V. D’Innocenzo, C. Tao, S. Pathak, H. J. Snaith, A. Petrozza, F. De Angelis, *Energy Environ. Sci.* **2016**, *9*, 155.
- [3] T. C. Sum, N. Mathews, *Energy Environ. Sci.* **2014**, *7*, 2518.
- [4] A. K. Jena, A. Kulkarni, T. Miyasaka, *Chem. Rev.* **2019**, *119*, 3036.
- [5] L. Lei, Q. Dong, K. Gundogdu, F. So, *Adv. Funct. Mater.* **2021**, *31*, 2010144.
- [6] K. Wang, C. Wu, Y. Hou, D. Yang, T. Ye, J. Yoon, M. Sanghadasa, S. Priya, *Energy Environ. Sci.* **2020**, *13*, 3412.
- [7] National Renewable Energy Laboratory, Best Research-Cell Efficiency Chart, <https://www.nrel.gov/pv/cell-efficiency.html> (accessed: July 2021).
- [8] Z. Yang, Y. Deng, X. Zhang, S. Wang, H. Chen, S. Yang, J. Khurgin, N. X. Fang, X. Zhang, R. Ma, *Adv. Mater.* **2018**, *30*, 1704333.
- [9] Z. Cheng, K. Liu, J. Yang, X. Chen, X. Xie, B. Li, Z. Zhang, L. Liu, C. Shan, D. Shen, *ACS Appl. Mater. Interfaces* **2019**, *11*, 34144.
- [10] Y. Xu, S. Xu, H. Shao, H. Jiang, Y. Cui, C. Wang, *Nanotechnology* **2018**, *29*, 235603.
- [11] L. Zhang, F. Yu, L. Chen, J. Li, *Appl. Surf. Sci.* **2018**, *443*, 176.
- [12] T. Leijtens, K. Bush, R. Checharoen, R. Beal, A. Bowring, M. D. McGehee, *J. Mater. Chem. A* **2017**, *5*, 11483.
- [13] R. Fu, Y. Zhao, Q. Li, W. Zhou, D. Yu, Q. Zhao, *Chem. Commun.* **2017**, *53*, 1829.
- [14] T. Leijtens, G. E. Eperon, N. K. Noel, S. N. Habisreutinger, A. Petrozza, H. J. Snaith, *Adv. Energy Mater.* **2015**, *5*, 1500963.
- [15] C. Zhang, T. Shen, D. Guo, L. Tang, K. Yang, H. Deng, *InfoMat* **2020**, *2*, 1034.
- [16] N. R. Poespawati, J. Sulistianto, T. Abuzairi, R. W. Purnamaningsih, *Int. J. Photoenergy* **2020**, *2020*, 8827917.
- [17] T. Wu, J. Li, Y. Zou, H. Xu, K. Wen, S. Wan, S. Bai, T. Song, J. A. McLeod, S. Duhm, F. Gao, B. Sun, *Angew. Chem., Int. Ed.* **2020**, *59*, 4099.
- [18] B. El Cohen, M. Wierzbowska, L. Etgar, *Adv. Funct. Mater.* **2017**, *27*, 1604733.
- [19] M. Dyksik, S. Wang, W. Paritmongkol, D. K. Maude, W. A. Tisdale, M. Baranowski, P. Plochocka, *J. Phys. Chem. Lett.* **2021**, *2*, 1638.
- [20] J. Qiu, Y. Xia, Y. Zheng, W. Hui, H. Gu, W. Yuan, H. Yu, L. Chao, T. Niu, Y. Yang, X. Gao, Y. Chen, W. Huang, *ACS Energy Lett.* **2019**, *4*, 1513.
- [21] C. Liang, H. Gu, Y. Xia, Z. Wang, X. Liu, J. Xia, S. Zuo, Y. Hu, X. Gao, W. Hui, L. Chao, T. Niu, M. Fang, H. Lu, H. Dong, H. Yu, S. Chen, X. Ran, L. Song, B. Li, J. Zhang, Y. Peng, G. Shao, J. Wang, Y. Chen, G. Xing, W. Huang, *Nat. Energy* **2021**, *6*, 38.
- [22] Z. Lai, Y. Meng, Q. Zhu, F. Wang, X. Bu, F. Li, W. Wang, C. Liu, F. Wang, J. C. Ho, *Small* **2021**, *17*, 2100442.
- [23] P. Chen, Y. Bai, S. Wang, M. Lyu, J. H. Yun, L. Wang, *Adv. Funct. Mater.* **2018**, *28*, 1706923.
- [24] J. Hu, L. Yan, W. You, *Adv. Mater.* **2018**, *30*, 1802041.
- [25] Z. Lai, R. Dong, Q. Zhu, Y. Meng, F. Wang, F. Li, X. Bu, X. Kang, H. Zhang, Q. Quan, W. Wang, F. Wang, S. Yip, J. C. Ho, *ACS Appl. Mater. Interfaces* **2020**, *12*, 39567.
- [26] L. Mao, W. Ke, L. Pedesseau, Y. Wu, C. Katan, J. Even, M. R. Wasielewski, C. C. Stoumpos, M. G. Kanatzidis, *J. Am. Chem. Soc.* **2018**, *140*, 3775.
- [27] S. Ahmad, P. Fu, S. Yu, Q. Yang, X. Liu, X. Wang, X. Wang, X. Guo, C. Li, *Joule* **2019**, *3*, 794.
- [28] X. Jiang, J. Zhang, S. Ahmad, D. Tu, X. Liu, G. Jia, X. Guo, C. Li, *Nano Energy* **2020**, *75*, 104892.
- [29] A. Dučinskas, G. Y. Kim, D. Moia, A. Senocrate, Y.-R. Wang, M. A. Hope, A. Mishra, D. J. Kubicki, M. Siczek, W. Bury, T. Schneeberger, L. Emsley, J. V. Milič, J. Maier, M. Grätzel, *ACS Energy Lett.* **2021**, *6*, 337.
- [30] Z. Fang, X. Hou, Y. Zheng, Z. Yang, K. C. Chou, G. Shao, M. Shang, W. Yang, T. Wu, *Adv. Funct. Mater.* **2021**, *1*, 2102330.
- [31] M. Koehl, M. Heck, S. Wiesmeier, J. Wirth, *Sol. Energy Mater. Sol. Cells* **2011**, *95*, 1638.
- [32] N. Klein-Kedem, D. Cahen, G. Hodes, *Acc. Chem. Res.* **2016**, *49*, 347.
- [33] G. W. P. Adhyaksa, S. Brittan, H. Āboliņš, A. Lof, X. Li, J. D. Keelor, Y. Luo, T. Duevski, R. M. A. Heeren, S. R. Ellis, D. P. Fenning, E. C. Garnett, *Adv. Mater.* **2018**, *30*, 1804792.
- [34] Y. Zhou, H. Sternlicht, N. P. Padture, *Joule* **2019**, *3*, 641.
- [35] O. Lopez-Sanchez, D. Lembke, M. Kayci, A. Radenovic, A. Kis, *Nat. Nanotechnol.* **2013**, *8*, 497.
- [36] C. Lan, C. Li, S. Wang, T. He, Z. Zhou, D. Wei, H. Guo, H. Yang, Y. Liu, *J. Mater. Chem. C* **2017**, *5*, 1494.
- [37] H. H. Fang, J. Yang, S. Tao, S. Adjokatse, M. E. Kamminga, J. Ye, G. R. Blake, J. Even, M. A. Loi, *Adv. Funct. Mater.* **2018**, *28*, 1800305.
- [38] B. Conings, J. Drijkoningen, N. Gauquelin, A. Babayigit, J. D’Haen, L. D’Olieslaeger, A. Ethirajan, J. Verbeeck, J. Manca, E. Mosconi, F. De Angelis, H. G. Boyen, *Adv. Energy Mater.* **2015**, *5*, 1500477.
- [39] A. Lemmerer, D. G. Billing, *CrystEngComm* **2012**, *14*, 1954.
- [40] S. K. Yadavalli, M. Chen, M. Hu, Z. Dai, Y. Zhou, N. P. Padture, *Scr. Mater.* **2020**, *187*, 88.
- [41] C. Xiao, Z. Li, H. Guthrey, J. Moseley, Y. Yang, S. Wozny, H. Moutinho, B. To, J. J. Berry, B. Gorman, Y. Yan, K. Zhu, M. Al-jassim, *J. Phys. Chem. C* **2015**, *119*, 26904.
- [42] Z. Fang, M. Shang, Y. Zheng, T. Zhang, Z. Du, G. Wang, X. Duan, K. C. Chou, C. H. Lin, W. Yang, X. Hou, T. Wu, *Mater. Horiz.* **2020**, *7*, 1042.